IEEE Access
Multidisciplinary | Rapid Review | Open Access Journal

IEEE POWER & ENERGY SOCIETY SECTION

Received October 18, 2020, accepted November 2, 2020, date of publication November 4, 2020,
date of current version November 25, 2020.

Digital Object Identifier 10.1109/ACCESS.2020.3035867

Improved Feeder Flow Control Method for a Virtual Power Plant With Various Resources to Reduce Communication Dependency

JAE-WON CHANG[1], (Student Member, IEEE), HEE SEUNG MOON[1], (Student Member, IEEE), SEUNG-IL MOON[1], (Senior Member, IEEE), YONG TAE YOON[1], (Member, IEEE), MARK B. GLICK[2], (Member, IEEE), AND SEUNG WAN KIM[3], (Member, IEEE)

[1]School of Electrical Engineering and Computer Science, Seoul National University, Seoul 08826, South Korea
[2]Hawaii Natural Energy Institute, University of Hawaii at Manoa, Honolulu, HI 96822, USA
[3]Department of Electrical Engineering, Chungnam National University, Daejeon 34134, South Korea

Corresponding author: Seung Wan Kim (swakim@cnu.ac.kr)

This work was supported in part by the Korea Institute of Energy Technology Evaluation and Planning (KETEP), in part by the Ministry of Trade, Industry and Energy (MOTIE) of the Republic of Korea (No. 20188550000410), and in part by the "Human Resources Program in Energy Technology" of the Korea Institute of Energy Technology Evaluation and Planning (KETEP), granted financial resource from the Ministry of Trade, Industry & Energy, Republic of Korea (No. 20194030202420).

ABSTRACT The concept of a virtual power plant (VPP) was introduced for supporting market participation of small-scale renewable energy-based generators (REGs). In a VPP, energy storage systems (ESSs) and micro-turbine-based generators (MTGs) are used together to mitigate the variability of the output of REGs. To keep the output of a VPP at the contracted value in a market, centralized feeder flow control (FFC) methods can be adopted for the VPP. However, conventional centralized FFC methods lack careful consideration of different characteristics of various resources and require high-speed communications and several central control units. Therefore, this paper proposes a new FFC method considering various characteristics of resources and enabling operation with less communication dependency. The effectiveness of the proposed method is verified by comparing the results of the proposed method with those of the conventional method with performance analysis, stability analysis, and simulations with Simulink/MATLAB.

INDEX TERMS Communication dependency, distributed energy resource, feeder flow control, robust stability, virtual power plant.

I. INTRODUCTION

Recently, a number of renewable energy-based generators (REGs), such as photovoltaic (PV) and wind generators, have been integrated into distribution networks to decarbonize energy systems [1]. However, the characteristics of REG, i.e., limited capacity and high output variability, hinder the achievement of ambitious national goal for greenhouse gas reduction by integration of REGs. As a generator must satisfy the minimum capacity requirement, limited capacity of REGs is an obstacle to the participation of REGs in the wholesale energy market to retain additional revenue streams [2]. Furthermore, the fluctuating output of REGs is the primary reason why there is a technical limit to their penetration in the current power system [3].

For these reasons, the concept of a virtual power plant (VPP) has been introduced to overcome these obstacles. A VPP aggregates a large number of REGs and manages multiple REGs as a single generator [3]. As aggregation of REGs as a VPP makes REGs possible to participate in the wholesale market, each REG can participate in the market for obtaining additional revenues. However, the output of a VPP is still difficult to be maintained as the desired value using only a collection of REGs [4]. For this reason, energy storage systems based on batteries (ESSs) are put into a portfolio of the VPP to mitigate variable outputs of REGs. However, as an ESS cannot discharge energy beyond its capacity, generators which can dynamically control their output, such as micro-turbine-based generators (MTGs), are additionally

The associate editor coordinating the review of this manuscript and approving it for publication was Guangya Yang.

required in the VPP to maintain the total output of the VPP at the desired value [5]. By coordinating distributed energy resources (DERs), such as REGs, ESSs, and MTGs, the VPP can procure enough capacity and cope with the variability of REGs as shown in Fig. 1.

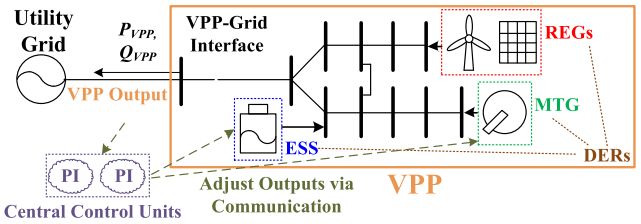

FIGURE 1. Structure of VPP and conventional centralized feeder flow control for VPP.

To keep the output of the VPP at the contracted value, feeder flow control (FFC) methods, which have been studied in [6]–[9], could be adopted. FFC methods make the power flow of specified feeder as desired using DERs. In a VPP, by utilizing controllable DERs, such as ESSs and MTGs, FFC methods can maintain the VPP output (i.e., VPP-Grid interface flow) as contracted value. In [6], a local control-based FFC method is proposed. Because this method is based on local control, FFC with a fast response time and high reliability can be implemented. However, this method is only applicable to small-scale radial networks. For applying FFC to general and larger networks, high-speed communication-based centralized FFC methods are proposed, as depicted in Fig. 1 [7]–[9]. By adopting the concept of the tie-line flow control in the conventional power system, central control units adjust the outputs of DERs to maintain the active power and reactive power of a VPP at the contracted values via high-speed communication.

While the conventional centralized FFC methods provide a way to control the VPP output, several factors should be further addressed. First, the different characteristics of various DERs need to be considered. As individual DERs have different characteristics, such as different response times and energy availability, the benefits of VPP are maximized if the characteristics of individual DERs can be considered. In microgrids (MGs), there are various studies that consider the different characteristics of various DERs [10]–[16]. For the operation of MGs, microgrid operators schedule the outputs of DERs with optimization while considering different response time of DERs [10]–[13]. For the control of MGs, considering the different characteristics of DERs, coordinated control of DERs has been proposed in [14]–[16]. Through such an approach, costs as well as losses of the system can be lowered and control performance can be improved in MGs. In the case of VPP, various studies, which considers the different characteristics of DERs, have been proposed for the operation of VPP and thus the cost and loss for the VPP can be lowered [17]–[19]. However, previous studies related to control methods including FFC for VPP scarcely consider the characteristics of DERs. Therefore, a coordinated control strategy considering the characteristics of individual DERs is required to maximize the benefit of each DER and performance of the control for VPP.

Second, the communication dependency of conventional methods needs to be reduced. As conventional centralized FFC methods use central PI control units, unexpected communication delay could seriously degrade the system stability [20]; thus, high-speed communication is essential for the conventional methods. Furthermore, as conventional FFC methods require at least two central control units for active power and reactive power controls, the system is exposed to serious risks of the failure of central control units [21]. Similar issues about communication dependency, such as the requirement for high-speed communication or the reduction of central control units, exist in MG or power system area. In [22] and [23], not to use high-speed communication, design methods for a central control unit have been proposed with fuzzy logics or robust control theory against an unexpected communication delay. However, these methods are proposed only for frequency and voltage control and scarcely consider the detailed dynamics of various DERs. On the other hand, in [24]–[26], to reduce the use of central control units, local-based control methods have been proposed. However, these methods can be used only for frequency and voltage control of MGs and can be adopted in only special topologies. Therefore, to reduce communication dependency in VPP, a novel robust control system for FFC in the VPP, which can function well even with an unexpected delay in communication speed and has less central units, is required.

In this paper, we propose an improved FFC method to maintain the output of VPP at a contracted value. The contributions of this paper are summarized as: 1) effective consideration of the different characteristics of various DERs and 2) reduction of communication dependency for FFC of VPP. The main proposals of this paper are as follows:

- Proposed centralized FFC structure for the active power control of VPP: considering different characteristics and response times for the various types of DERs, better performing centralized FFC structure for the active power control of VPP is proposed.
- Gain design method of the FFC for the active power control of VPP: to reduce communication dependency, control gain design method of proposed FFC for active power control of VPP, which makes the system stable against unexpected communication delay, is introduced.
- Proposed local FFC method for the reactive power control of VPP: local FFC method for the reactive power control of VPP is proposed in each DER to reduce the use of central control unit.

The remainder of this paper is organized as follows. In Section II, various types of DERs in a VPP are analyzed for categorization and equivalent modeling. In Section III, a conventional centralized FFC method is reviewed. In Section IV, the proposed FFC method for control of the VPP output is presented. In Section V, we present the results of the analysis and simulations, and thus validate the effectiveness of the

proposed control method. Finally, conclusions are outlined in Section VI.

II. CLASSIFICATION AND ANALYSIS OF DERS IN VPP

As there are various types of DERs in a VPP, the characteristics of individual DERs are required to be analyzed for efficient coordination among DERs. In this section, the different types of DERs are analyzed. Based on the implementation method and source type, we can categorize DERs, which have been widely used in VPP, into three types: REG, ESS, and MTG. In addition, a simplified equivalent model of DERs is presented.

A. CLASSIFICATION OF DERs IN VPP

1) REG

Owing to having eco-friendly characteristics, REGs such as wind and PV generators are in the spotlight as future power generation sources. Most REGs are integrated into the power system through an inverter as shown in Fig. 2(a). For maximizing the use of renewable energy sources, an REG is generally controlled for the maximum power point tracking (MPPT) by the inverter control [27]. However, as the available power from REGs, such as PV and wind power generators, is uncertain and fluctuates, there are major factors that create uncertainty and volatility of VPP output.

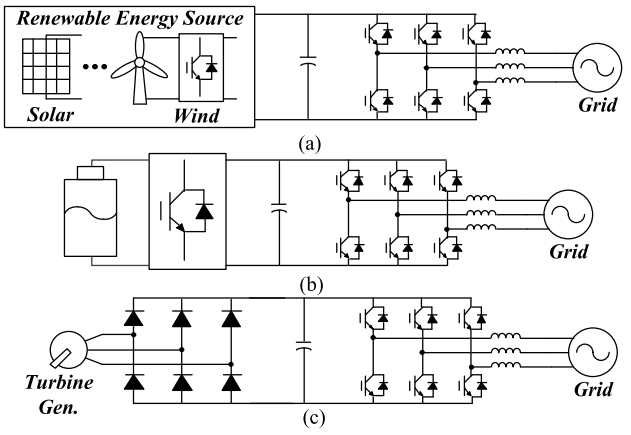

FIGURE 2. Structure of grid interfaced DER; (a) REG, (b) ESS, and (c) MTG.

2) ESS

An ESS consists of a battery (i.e., a power source) and an inverter that is required for interfacing a battery to the power system as shown in Fig. 2(b) [15]. As the output of an ESS can be controlled by an inverter, an ESS can be used to mitigate the variable outputs of REGs and maintain the VPP output at the contracted value. Furthermore, because an ESS is usually based on a Li-ion battery source that has a fast response time of less than 1 ms [28], the bandwidth of an inverter controller can be large; hence, the ESS has a very fast response time. Generally, the bandwidth of the power controller for an ESS could be over a thousand [15]. However, an ESS has a state of charge (SOC) limitation due to the battery capacity. Therefore, thorough SOC management for an ESS is essential [15].

3) MTG

MTGs consist of a micro-turbine and ac generator to generate electrical power from various fuel-based sources [29]. Many conventional fuel sources have been adapted to MTGs. However, biomass and natural gas can be sources for MTGs to reduce pollution. MTGs recently have been interfaced to the power system through converters for high efficiency and fast operation [29]. The most common converter topology is the back-to-back converters that consist of a dc–link, a rectifier, and an inverter. The entire scheme of the grid-interfaced MTG is expressed in Fig. 2(c). For mitigating variable outputs of REGs, MTGs are required and a stable power supply of VPP is possible. Different from an ESS, the outputs can be managed more easily without a constraint, such as SOC [15]. However, the response time of MTG is relatively slow [15]. Although each MTG is interfaced to the system by inverter, the bandwidth of the inverter controller is limited due to the slow response of the prime mover when compared to a battery [30]. Generally, the bandwidth of the power controller for an MTG is limited, about a hundred [31].

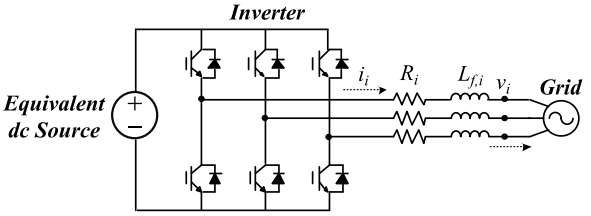

FIGURE 3. Equivalent system of each DER.

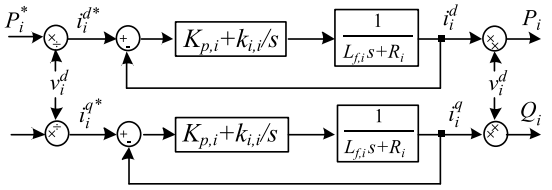

FIGURE 4. Control structure of each DER.

B. EQUIVALENT MODEL OF DERS IN VPP

As analyzed above, we assume all DERs are interfaced to the system via inverters. From [15], [27], [30], [31], all REG, ESS, and MTG can be seen as equivalent to a structure that includes a dc voltage source and an inverter when viewed from the perspective of the grid as shown in Fig. 3. Fig. 4 shows the inverter controllers within the system in Fig. 3. The purpose of the controllers is to regulate the power at their reference values. When * denotes the reference of a corresponding variable, all references become the optimal scheduled values provided by the operator in steady-state, but the active power reference of REG becomes the power at MPP (P_{MPPT}) [27]. The PI gains of the current controller are expressed as $k_{p,i}$ and $k_{i,i}$.

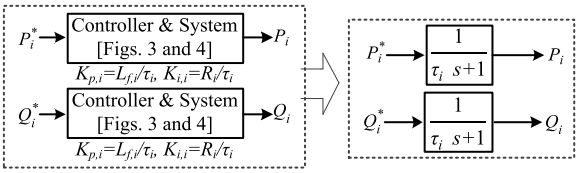

FIGURE 5. Equivalent model of each DER.

Fig. 5 shows the procedure for expressing the equivalent model for DERs. If $k_{p,i}$ and $k_{i,I}$ are determined as $k_{p,I} = L_{f,i}/\tau_i$ and $k_{i,I} = R_i/\tau_i$, the DER (which consists of the system in Fig. 3 and controller in Fig. 4) can be expressed as a first-order low pass filter (LPF) with time constant of τ_i [32]. Finally, the DER can be simplified as a single transfer function. Note that the different types of DERs have different values for τ_i, which corresponds to the response time and is the reciprocal of the bandwidth.

III. CONVENTIONAL CENTRALIZED FEEDER FLOW CONTROL FOR VPP

If the actual outputs of REGs are changed from the predicted values, the real-time output of the VPP develops an error from the contracted value. To compensate for the error, the VPP output can be maintained at a contracted value by adopting the conventional centralized FFC method, as shown in Fig. 6 [7]–[9]. The errors between the actual outputs, P_{VPP} and Q_{VPP}, and the contracted output values, $P_{VPP,0}$ and $Q_{VPP,0}$, become the inputs of the central PI controllers, where k_p and k_i are the gains of the central PI controllers. Then, the output of the central PI controller for the active power becomes the total adjusted references of controllable DERs, such as MTGs and ESSs. On the other hand, the central controller for the reactive power becomes the total adjusted references of all DERs, including REGs. The output signals of the central PI controllers are distributed via high-speed communication to each DER based on the sharing ratio. Normally, the sharing ratio can be determined equally or based on the rating ratio [27]. Finally, the signals become the adjusted references for the active and reactive powers of each DER.

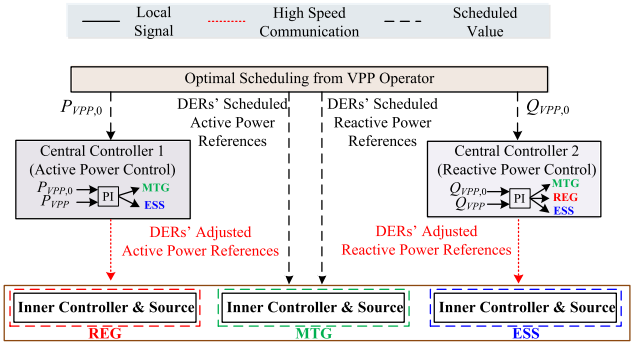

FIGURE 6. Entire structure of conventional centralized FFC for VPP.

IV. PROPOSED FEEDER FLOW CONTROL FOR VPP

Conventional centralized FFC methods have some drawbacks as mentioned in Section I. Different characteristics of each DER are not considered. Furthermore, these methods have high communication dependency, such as the requirement of high-speed communication and multiple central control units for the active and reactive power control. Therefore, in this paper, an improved FFC method is proposed for the active and reactive power control of the VPP output, as shown in Fig. 7. For the active power control of a VPP, considering different characteristics of the DERs and any unexpected delay in communication, the structure of the conventional centralized FFC is modified and a gain design method is introduced. For the reactive power control of a VPP, instead of using a central controller, a local-based reactive power controller in each DER is proposed to reduce the use of central control unit.

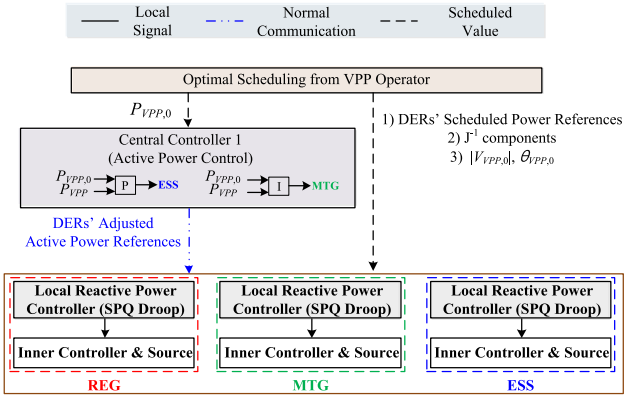

FIGURE 7. Entire structure of proposed FFC for VPP.

A. PROPOSED FFC METHOD FOR THE ACTIVE POWER CONTROL OF VPP

1) MODIFIED STRUCTURE OF CENTRALIZED CONTROL

As ESSs have fast response times but should manage SOC thoroughly, it is desirable that ESSs participate in instant control rather than steady-state control [15]. MTGs, on the other hand, have relatively slow response times but have no restrictions like the SOC limitation, making it relatively easy to adjust their outputs [15]. In the active power control of a VPP, a central controller is used, as in conventional methods. However, considering the characteristics of ESSs, the control signal from the P controller is assigned to the ESSs. The P controller adjusts the output instantaneously to compensate for the error but returns the output to zero when the error becomes zero. Similarly, the control action of the I controller is assigned to MTGs. The I controller adjusts the output slowly for eliminating the error, and the output becomes a different value from the base points even when the error becomes zero. If there are multiple ESSs and MTGs, the control signals for ESSs and MTGs are allocated to each ESS and MTG via sharing ratios, $pf_{ESS,i}$ and $pf_{MTG,j}$, of which their summation is equal to one, respectively. At last, the signals become the adjusted active power references of ESSs and MTGs. Fig. 8 shows the entire active power control loops considering the transfer function of communication and

responses of MTGs and ESSs as analyzed in Fig. 5. The communication speed model is approximated as the LPF form as expressed in [20]. For simplification, the time constant of the communication speed is equal to τ_d in all links and the time constants for MTGs and ESSs are equal to τ_{ESS} and τ_{MTG}, respectively.

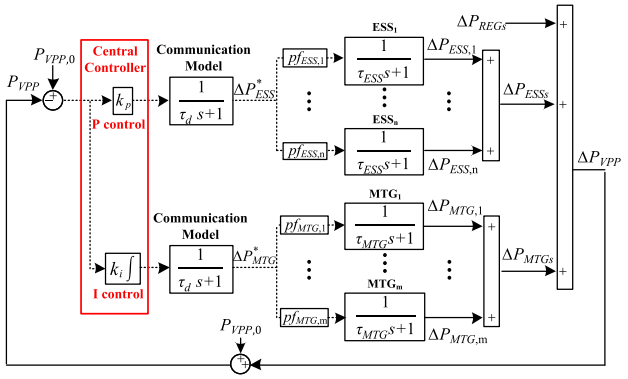

FIGURE 8. Entire loop of the proposed FFC for active power of VPP.

2) SMALL-SIGNAL-BASED STATE SPACE MODEL

For designing the gains for the central active power controller and verifying the system stability, a small-signal-based state space model is presented. Assuming that the loss in the system is negligible and that a VPP consists of REGs, MTGs, and ESSs, as shown in Fig. 1, the following equation can be satisfied from the power balance equation.

$$\Delta P_{VPP} = \Delta P_{MTGs} + \Delta P_{ESSs} + \Delta P_{REGs}, \tag{1}$$

where Δ denotes the variation of corresponding variable and P_{VPP}, P_{MTGs}, P_{ESSs}, and P_{REGs} are the active power of VPP, MTGs, ESSs, and REGs, respectively. From Fig. 8, the relationship between ΔP_{VPP} and ΔP^*_{ESSs} can be expressed as follow:

$$-k_p \Delta P_{VPP} = \tau_d \Delta \dot{P}^*_{ESSs} + \Delta P^*_{ESSs}, \tag{2}$$

where * denotes the reference of corresponding variables. Considering that the summation of participation factors is one in Fig. 8, the relationship between ΔP^*_{ESSs} and ΔP_{ESSs} can be written as:

$$\Delta P^*_{ESSs} = \tau_{ESS} \Delta \dot{P}_{ESSs} + \Delta P_{ESSs}. \tag{3}$$

Similarly, the relationships between ΔP_{VPP} and ΔP^*_{MTGs} and between ΔP^*_{MTGs} and ΔP_{MTGs} can be presented as:

$$-k_i \Delta P_{VPP} = \tau_d \Delta \ddot{P}^*_{MTGs} + \Delta \dot{P}^*_{MTGs}, \tag{4}$$

$$\Delta P^*_{MTGs} = \tau_{MTG} \Delta \dot{P}_{MTGs} + \Delta P_{MTGs}. \tag{5}$$

On the other hand, P_{REGs} can be considered as the input of the system. From (1)–(5), the entire state space model of the system including the central controller, communication, and responses of MTGs, ESSs, and REGs can be expressed as (6) and (7).

$$\dot{\mathbf{X}} = \mathbf{AX} + \mathbf{BU}, \tag{6}$$

$$\mathbf{Y} = \mathbf{CX}, \tag{7}$$

where,

$$\mathbf{X} = [\Delta P_{VPP}, \Delta P_{MTGs}, \Delta \dot{P}_{MTGs}, \Delta \ddot{P}_{MTGs}, \Delta P_{ESSs}, \Delta \dot{P}_{ESSs}]^T,$$

$$\mathbf{U} = [\Delta \dot{P}_{REGs}], \quad \mathbf{Y} = [\Delta P_{VPP}],$$

$$\mathbf{A} = \begin{bmatrix} 0 & 0 & 1 & 0 & 0 & 1 \\ 0 & 0 & 1 & 0 & 0 & 0 \\ 0 & 0 & 0 & 1 & 0 & 0 \\ a_1 & 0 & a_2 & a_3 & 0 & 0 \\ 0 & 0 & 0 & 0 & 0 & 1 \\ a_4 & 0 & 0 & 0 & a_5 & a_6 \end{bmatrix},$$

$$\mathbf{B} = \begin{bmatrix} 1 \\ 0 \\ 0 \\ 0 \\ 0 \\ 0 \end{bmatrix}, \quad \mathbf{C} = \begin{bmatrix} 1 \\ 0 \\ 0 \\ 0 \\ 0 \\ 0 \end{bmatrix}^T,$$

$$a_1 = -k_i \tau_d^{-1} \tau_{MTG}^{-1}, a_2 = k_i^{-1} a_2, a_3 = (\tau_d + \tau_{MTG}) a_5.$$

$$a_4 = -k_p \tau_d^{-1} \tau_{ESS}^{-1}, a_5 = k_p^{-1} a_4, a_6 = (\tau_d + \tau_{ESS}) a_5.$$

3) DESIGN METHOD OF THE CONTROLLER GAINS

The central controller gains critically affect system stability and performance. Conventionally, PI gains of the central controller are optimally designed at the nominal condition of the system. Heuristic optimization methods have been widely adopted for the design of gains, such as the genetic algorithm (GA) [33] and the particle swarm optimization (PSO) [34]. In this paper, PSO is selected for the optimization tool, and the previous optimal design method of PI gains is adopted to obtain the best performance. The P gain and I gain, k_p and k_i, in the central active power controller are determined for minimizing the objective function $f(\mathrm{x})$ as

$$\min f(x) = \int_{t=0}^{t=T} t \cdot |P_{VPP}(t) - P_{VPP,0}| dt, \tag{8}$$

where $f(\mathrm{x})$ implies the integrated time-weighted absolute error (ITAE) between the actual VPP output and the contracted value. ITAE is well-known as the objective function which yields the best performance indicator [34]. From the optimization for the simulation results of the state space model in (6) and (7) with the step change of input, the optimal gains can be obtained in a similar way to the previous studies [33], [34].

However, in this paper, we want to use normal communication lines, instead of high-speed communication lines, to reduce communication dependency. In this case, unexpected communication delays inevitably occur. For this reason, the gains should be designed to guarantee system stability even if the unexpected communication delay occurs. To prevent instability due to the uncertainty, robustness against the unexpected delay should be considered in the design of the gains. The uncertainties of communication speed can be modeled as an inverse additive perturbation [35], [36]. The general structure of the closed-loop system with the inverse additive perturbation is shown in Fig. 9.

A necessary and sufficient condition for robust stability against the uncertainty is [37]

$$||\mathbf{M} \cdot \Delta||_\infty < 1, \tag{9}$$

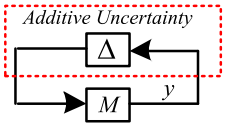

FIGURE 9. Closed loop with an additive uncertainty of communication speed.

From (6) and (7), a closed-loop system $\mathbf{M}$ can be obtained as

$$\mathbf{M} = \mathbf{C}(s\mathbf{I} - \mathbf{A})^{-1}\mathbf{B}, \tag{10}$$

Considering the form of the transfer function for the communication in Fig. 8, we can express the uncertainty as

$$||\Delta(\omega)||_\infty < 1, \tag{11}$$

Based on small-gain theorem [37], $\mathbf{M}$ should be satisfied with the following condition to maintain robust stability.

$$||\mathbf{M}||_\infty < 1, \tag{12}$$

Thus, to guarantee the robust stability for uncertainty, (12) becomes a constraint of the optimization to design the gains.

B. PROPOSED FFC METHOD FOR THE REACTIVE POWER CONTROL OF VPP

1) LOCAL-BASED SPQ DROOP CONTROL

As the reactive power could be controlled by the inverter of each DER regardless of source types, it seems that the reactive power of a VPP output is almost unchanged. However, if the active power of a DER changes, the reactive power of the VPP could be changed by the variation in the power flow through the lines [38]. For this reason, as the active power of all DERs could be changed unexpectedly from the scheduled value, effective reactive power control for the VPP output should also be required. Conventionally, similar to the active power control, a PI-based central controller is adopted for FFC of the reactive power control [7]–[9]. However, considering that use of fewer central control units is preferred from the standpoint of system reliability [20], we propose a local reactive power control method to maintain the reactive power of a VPP as desired in this section.

The main concept of the proposed reactive power control of a VPP is as follows. The output of an REG can vary from the base point due to a change in the available active power, and the outputs of ESSs and MTGs can also vary from the base points due to their participation in the active power control. While DERs adjust their active powers from the base points, the corresponding DERs compensate for the reactive powers simultaneously to suppress the variation in the reactive power of the VPP. To compensate, sensitivity based active–reactive power (SPQ) droop control is proposed.

Considering that the base point is determined by the operator with the optimal scheduling, the base points of the active and reactive powers for each DER and the reactive power for VPP are expressed as $P_{DER,0}$, $Q_{DER,0}$, and $Q_{VPP,0}$ respectively. If the active power of the DER deviates from the base point, the variation in the active power for the DER is expressed as ΔP_{DER}. As mentioned above, ΔP_{DER} can affect the variation of Q_{VPP}. Assuming the outputs of other DERs are not changed, the variation in Q_{VPP} can be expressed as follows.

$$\Delta Q_{VPP} = \frac{\partial Q_{VPP,0}}{\partial P_{DER,0}}\Delta P_{DER} + \frac{\partial Q_{VPP,0}}{\partial Q_{DER,0}}\Delta Q_{DER}, \tag{13}$$

where Δ denotes the variation of the corresponding variable. Therefore, to maintain ΔQ_{VPP} at zero in (13), the variation of required reactive power of DER, ΔQ_{DER}, can be written as

$$\Delta Q_{DER} = K_{SPQ}\Delta P_{DER}, \tag{14}$$

$$\begin{aligned} K_{SPQ} &= -\left(\frac{\partial Q_{VPP,0}}{\partial P_{DER,0}}\right) \cdot \left(\frac{\partial Q_{VPP,0}}{\partial Q_{DER,0}}\right)^{-1} \\ &= -im\left(\frac{\partial S_{VPP,0}}{\partial P_{DER,0}}\right) \cdot im\left(\frac{\partial S_{VPP,0}}{\partial Q_{DER,0}}\right)^{-1}, \end{aligned} \tag{15}$$

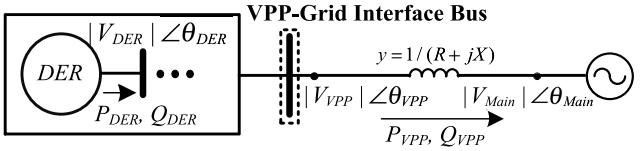

FIGURE 10. Simplified structure of VPP interface with a utility gird.

where K_{SPQ} is the droop constant for SPQ droop control, which is expressed by sensitivities. If K_{SPQ} can be estimated, the variation of Q_{VPP} could be suppressed locally from each DER by adjusting its reactive power. For estimating K_{SPQ}, sensitivities between the apparent power of VPP and $P_{DER,0}$ and $Q_{DER,0}$ are required. Fig. 10 shows the interface of VPP, which is connected to the main grid with the impedance. From Fig. 10, the apparent power of VPP, S_{VPP}, is expressed as

$$S_{VPP} = -V_{Main} \cdot [y \cdot (V_{Main} - V_{VPP})]^*, \tag{16}$$

where V_{Main} is the voltage of the main grid, V_{VPP} is the voltage for the VPP-Grid interface bus, and y is the admittance between the main grid and the VPP. By partial differentiation of (16) to the active and reactive power of DER, the following sensitivities are written as

$$\begin{aligned} \frac{\partial S_{VPP,0}}{\partial P_{DER,0}} &= -V_{Main} y \left[\left(\frac{\partial V_{Main}}{\partial P_{DER,0}}\right) - \left(\frac{\partial V_{VPP,0}}{\partial P_{DER,0}}\right)\right]^* \\ &\quad + y\frac{\partial V_{Main}}{\partial P_{DER,0}}(V_{Main} - V_{VPP})^*, \end{aligned} \tag{17}$$

$$\begin{aligned} \frac{\partial S_{VPP,0}}{\partial Q_{DER,0}} &= -V_{Main} y \left[\left(\frac{\partial V_{Main}}{\partial Q_{DER,0}}\right) - \left(\frac{\partial V_{VPP,0}}{\partial Q_{DER,0}}\right)\right]^* \\ &\quad + y\frac{\partial V_{Main}}{\partial Q_{DER,0}}(V_{Main} - V_{VPP})^*. \end{aligned} \tag{18}$$

From the perspective of the VPP, as the main grid can be thought of as an infinite bus, the voltage magnitude and angle

are assumed as 1 p.u. and 0 rad, respectively. Thus, y can be known, hence, (17) and (18) can be re-expressed as

$$\frac{\partial S_{VPP,0}}{\partial P_{DER,0}} = \left[y\left(\frac{\partial V_{VPP,0}}{\partial P_{DER,0}}\right)\right]^*, \tag{19}$$

$$\frac{\partial S_{VPP,0}}{\partial Q_{DER,0}} = \left[y\left(\frac{\partial V_{VPP,0}}{\partial Q_{DER,0}}\right)\right]^*. \tag{20}$$

Therefore, to estimate K_{SPQ}, the sensitivities between the VPP-Grid interface bus voltage and the active and reactive power of each DER should be known. From [39], the required sensitivities to estimate K_{SPQ} can be written as

$$\begin{aligned}\frac{\partial V_{VPP,0}}{\partial P_{DER,0}} &= \frac{\partial(|V_{VPP,0}| \cdot e^{j\theta_{VPP,0}})}{\partial P_{DER,0}} \\ &= \left[\frac{\partial |V_{VPP,0}|}{\partial P_{DER,0}} + j|V_{VPP,0}|\frac{\partial \theta_{VPP,0}}{\partial P_{DER,0}}\right] e^{j\theta_{VPP,0}}, \end{aligned} \tag{21}$$

$$\begin{aligned}\frac{\partial V_{VPP,0}}{\partial Q_{DER,0}} &= \frac{\partial(|V_{VPP,0}| \cdot e^{j\theta_{VPP,0}})}{\partial Q_{DER,0}} \\ &= \left[\frac{\partial |V_{VPP,0}|}{\partial Q_{DER,0}} + j|V_{VPP,0}|\frac{\partial \theta_{VPP,0}}{\partial Q_{DER,0}}\right] e^{j\theta_{VPP,0}}, \end{aligned} \tag{22}$$

where $|V_{VPP,0}|$ and $\theta_{VPP,0}$ are the voltage and angle magnitudes for the VPP-Grid interface bus. To estimate K_{SPQ}, as written in (15) and (19)–(22), information regarding $|V_{VPP,0}|$, $\theta_{VPP,0}$, and the four sensitivities, which are the components of the inverse of the Jacobian matrix, is required. Fortunately, those are calculated during the optimal scheduling and can be given by the operator without any extra process [39]. Finally, we can estimate K_{SPQ} from the scheduled data.

On the other hand, considering that the output of each DER is fluctuated with the variable outputs of REGs, voltage fluctuation can occur. Although the reactive power of DER is used to control the reactive power of VPP in the proposed control, a voltage should be maintained within the allowable range. If a voltage deviates away from the allowable range, the reactive power of DER should be adjusted to control its voltage instead of controlling the VPP output.

Considering that the base point is determined by the operator with optimal scheduling, the base points of the active and reactive powers for each DER and its voltage are expressed as $P_{DER,0}$, $Q_{DER,0}$, and $|V_{DER,0}|$, respectively. If the active power of the DER deviates from the base point, the variation in the active power for the DER, ΔP_{DER}, can affect the variation of $|V_{DER}|$. Therefore, the variation in $|V_{DER}|$ can be expressed as follows.

$$\Delta|V_{DER}| = \frac{\partial |V_{DER,0}|}{\partial P_{DER,0}}\Delta P_{DER} + \frac{\partial |V_{DER,0}|}{\partial Q_{DER,0}}\Delta Q_{DER}, \tag{23}$$

where Δ denotes the variation of the corresponding variable. If the proposed SPQ droop control with K_{SPQ} operates, the variation in the reactive power of DER can be expressed as

$$\Delta Q_{DER} = K_{SPQ}\Delta P_{DER}. \tag{24}$$

By substituting (24) into (23), the variation in $|V_{DER}|$ due to the proposed SPQ droop control can be estimated as

$$\Delta|V_{DER}| = \left(\frac{\partial |V_{DER,0}|}{\partial P_{DER,0}} + K_{SPQ}\right)\Delta P_{DER}. \tag{25}$$

As the actual voltage $|V_{DER}|$ is the summation of (25) and $|V_{DER,0}|$, $|V_{DER}|$ can be expressed as

$$|V_{DER}| = |V_{DER,0}| + \left(\frac{\partial |V_{DER,0}|}{\partial P_{DER,0}} + K_{SPQ}\right)\Delta P_{DER}. \tag{26}$$

However, if $|V_{DER}|$ deviates away from the allowable range as expressed in (27), the reactive power of DER should be used to control its voltage instead of controlling for the VPP output as mentioned above.

$$\begin{aligned}|V_{\min}| < |V_{DER}| = |V_{DER,0}| + \Big(&\frac{\partial |V_{DER,0}|}{\partial P_{DER,0}} \\ &+ K_{SPQ}\Big)\Delta P_{DER} < |V_{\max}|, \end{aligned} \tag{27}$$

where $|V_{min}|$ and $|V_{max}|$ are the minimum and maximum voltages of the allowable range. Fortunately, by changing the droop constant from the proposed SPQ droop constant, K_{SPQ}, to the supplementary SPQ droop constant, K'_{SPQ}, voltage can be recovered to the scheduled value. The concept of supplementary SPQ droop constant is based on the PQ droop control in [14]. When (27) is not satisfied, to make $\Delta|V_{DER}|$ as zero in (23), the variation of the required reactive power of DER, ΔQ_{DER}, can be expressed as

$$\Delta Q_{DER} = K'_{SPQ}\Delta P_{DER}, \tag{28}$$

$$K'_{SPQ} = -\left(\frac{\partial |V_{DER,0}|}{\partial P_{DER,0}}\right)\left(\frac{\partial |V_{DER,0}|}{\partial Q_{DER,0}}\right)^{-1}. \tag{29}$$

where K'_{SPQ} is the supplementary SPQ droop constant for voltage control, which is expressed by sensitivities. Therefore, if the DER adjusts the reactive power as (28) with K'_{SPQ}, the voltage fluctuation can be suppressed. To estimate K'_{SPQ}, sensitivities in (29) are required. Fortunately, as the sensitivities are the components for inverse of the Jacobian matrix, these sensitivities can be given during the scheduling and K'_{SPQ} are easily calculated without any additional process.

On the other hand, Jacobian matrix components are given from the operator and are used to estimate droop constants K'_{SPQ} and K'_{SPQ}. Thus, the uncertainties related to the power system may cause incorrect information of Jacobian matrix and it may degrade the control performance. Considering this case, the operator should estimate the Jacobian accurately even with the uncertainties. Fortunately, as Jacobian matrix is widely used for control, operation, and planning phases in power systems [40], [41], several studies emphasize the importance of estimation of Jacobian matrix with the uncertainties and propose a method to estimate Jacobian matrix [42], [43]. In [42], a measurement-based estimation method for Jacobian matrix is proposed using phasor measurement units (PMUs) and linear total least-squares algorithm even if uncertainties about the measurement error or the system topology occurs. On the other hand, [43] proposes an estimation method for the Jacobian matrix in ambient conditions using covariance-based statistical methods. Different

from [42], the system dynamic matrix can be also obtained in [43]. Using these methods from the operator, Jacobian matrix could be estimated in near real time even with uncertainties, such as measurement errors and network topology changes. In other words, it is possible to improve the robustness for the proposed control if such estimation methods for Jacobian matrix are used.

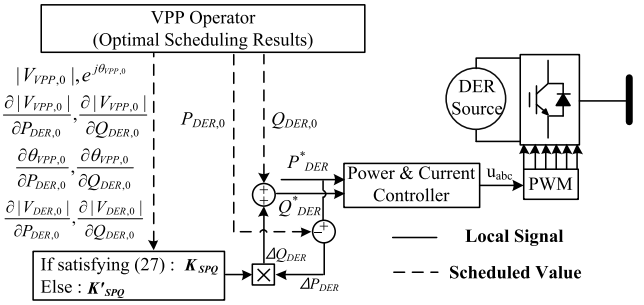

FIGURE 11. The proposed FFC for reactive power of VPP: SPQ droop-based local controller for each DER.

Finally, the entire proposed SPQ droop control is expressed as shown in Fig. 11. If the condition of (27) is satisfied, it is judged as normal state and the reactive power of DER is adjusted by multiplying the deviated active power and the proposed SPQ droop constant, K_{SPQ}. However, if the condition of (27) is not satisfied, it is judged as voltage abnormal state and the reactive power of DER is adjusted by multiplying the deviated active power and the supplementary SPQ droop constant, K'_{SPQ}. From the entire proposed SPQ droop control, the reactive power of VPP can be maintained locally in normal situation. However, if the voltage deviates away from the allowable range, the voltage returns to the scheduled value locally instead of maintaining the reactive power of VPP.

C. ENTIRE SCHEME OF THE PROPOSED FFC

The entire process of the proposed FFC for the VPP is summarized as shown in Fig 7. For active power control, the control structure is modified from the conventional centralized FFC method to consider the different characteristics of various DERs. Furthermore, the design method for control gains is proposed. Different from the conventional method in Fig. 6, normal communication lines can be used instead of high-speed communication lines.

Simultaneously, for reactive power control, SPQ droop controller in each DER is proposed for local FFC. Owing to the proposed reactive power control method, no central controller is required for reactive power control of the VPP. Finally, from the proposed FFC method, the VPP can reduce the overall communication dependency.

V. ANALYSIS AND SIMULATION RESULTS

In this section, analysis and simulation results with the proposed FFC method are compared to those with the conventional control method. The central PI controller-based method which has been widely used for the centralized FFC methods [7]–[9] was selected as the conventional control method. Furthermore, in the conventional method, we assume that the FFC signals are evenly allocated to MTG and ESS as the conventional way [27].

Firstly, the configuration of the test system is introduced. Based on the test system, the improvement of the proposed FFC for the active power of a VPP is verified with the analysis of performance and stability. The analysis of both performance and stability is performed based on the small-signal based state space models. The model of the proposed method is presented in (6) and (7) and the model of the conventional method is presented in Appendix A. After the analysis of the active power control method, time-domain simulations of a case study are performed to verify the effectiveness of the entire FFC method for a VPP.

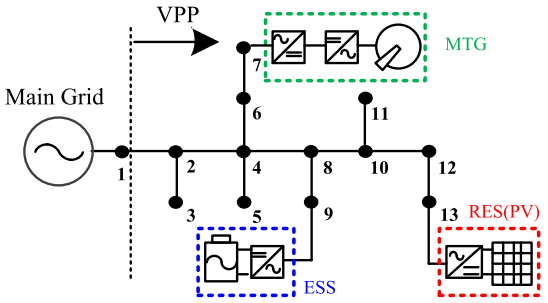

FIGURE 12. Test VPP system based on CIGRE benchmark model.

TABLE 1. System parameters at nominal condition.

Symbol	Value	Symbol	Value	Symbol	Value
$P_{VPP,0}$	60 kW	$Q_{VPP,0}$	30 kVar	$P_{ESS,0}$	20 kW
$Q_{ESS,0}$	10 kVar	$P_{MTG,0}$	11.59 kW	$Q_{MTG,0}$	9.69 kVar
$P_{REG,0}$	30 kW	$Q_{REG,0}$	15 kVar	$\lvert V_{VPP,0}\rvert$	1.026 p.u.
$\lvert\theta_{VPP,0}\rvert$	0.041 rad	$\frac{\partial\lvert V_{VPP,0}\rvert}{\partial P_{MTG,0}}$	0.0079	$\frac{\partial\lvert V_{VPP,0}\rvert}{\partial Q_{MTG,0}}$	0.2971
$\frac{\partial\lvert V_{VPP,0}\rvert}{\partial P_{ESS,0}}$	0.0072	$\frac{\partial\lvert V_{VPP,0}\rvert}{\partial Q_{ESS,0}}$	0.2974	$\frac{\partial\lvert V_{VPP,0}\rvert}{\partial P_{REG,0}}$	0.0041
$\frac{\partial\lvert V_{VPP,0}\rvert}{\partial Q_{REG,0}}$	0.2973	$\frac{\partial\theta_{VPP,0}}{\partial P_{MTG,0}}$	0.2785	$\frac{\partial\theta_{VPP,0}}{\partial Q_{MTG,0}}$	-0.0408
$\frac{\partial\theta_{VPP,0}}{\partial P_{ESS,0}}$	0.2767	$\frac{\partial\theta_{VPP,0}}{\partial Q_{ESS,0}}$	-0.0409	$\frac{\partial\theta_{VPP,0}}{\partial P_{RES,0}}$	0.2713
$\frac{\partial\theta_{VPP,0}}{\partial Q_{RES,0}}$	-0.0437	$K_{SPQ(\mathrm{MTG})}$	0.0937	$K_{SPQ(\mathrm{REG})}$	0.0951
$K_{SPQ(\mathrm{ESS})}$	0.103	$K'_{SPQ(\mathrm{MTG})}$	-0.483	$K'_{SPQ(\mathrm{REG})}$	-0.496
$K'_{SPQ(\mathrm{ESS})}$	-0.317	τ_{REG}	1 ms	τ_{ESS}	1 ms
τ_{MTG}	10 ms	τ_d	20 ms	-	-

A. SYSTEM CONFIGURATION

The VPP system shown in Fig. 12 was used as the test system with nominal parameters listed in Table 1. The test system was based on CIGRE low voltage benchmark system in [44] and some modification was adopted for making the system as VPP. At bus 7, 9, and 13, MTG, ESS, and REG (PV) were

connected, respectively. The detailed inner control scheme of each DER was adopted as depicted in Fig. 4. All inverters were two-level half bridge converters and were connected to the system with an RL filter ($R = 0.1$ mΩ, $L = 2$ mH). PI gains of the inner-loop inverter controller for MTG, ESS, and REG (PV) were designed to have time constants of $\tau_{MTG} = 10$, $\tau_{ESS} = 1$, and $\tau_{RES} = 1$ ms, respectively. Rated values for the apparent power of MTG, ESS, and REG were 50, 40, and 50 kVA, respectively.

On the other hand, it is assumed that the VPP operator contracted the power as 60 kW+ 30 kVar with the main grid and the active power of the REG was predicted as 30 kW. From the contracted power of the VPP with the main grid and the predicted power of the REG, the operator scheduled the active power and reactive power of each DER as shown in Table 1. From the scheduling, the base points and sensitivities were determined as shown in Table 1.

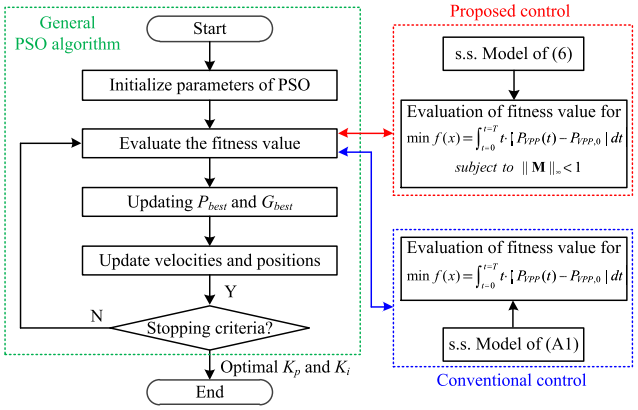

FIGURE 13. Flowchart of gain design process for the proposed and conventional control methods.

For an accurate comparison between the proposed control method and the conventional control method, the entire verification was carried out using the same methodology under the same conditions; with the unit step response of the system input (the output of REG), the gains for the central controller were optimally designed as conventional gain design methods [33], [34] to obtain the best performance by minimizing the objective function, (8). However, as proposed in Section IV-A, the constraint related to the robust stability in (12) was additionally considered in the design for the proposed case. PSO was adopted for the optimization tool in both methods. Fig. 13 shows the flowchart for the gain design process for the conventional and proposed methods. The population size of particles was chosen to be 10, the boundary of the gains was confined as (0 100,000), and a penalty constant was set to 100,000. From the optimization, the gains for the conventional and the proposed central controllers were designed as [1.7, 677] and [1, 37], respectively, under the same conditions. Fig. 14 shows the results of the PSO searching process in both methods. The values of the objective functions were saturated and minimized within 50 iterations.

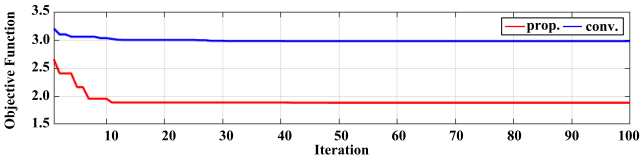

FIGURE 14. PSO convergence characteristics.

B. PERFORMANCE AND STABILITY ANALYSIS

The performance and the stability of the proposed FFC method for the active power control of a VPP were compared with those of the conventional method. The performance of both methods could be compared through the results from the objective functions shown in Fig. 14. As shown in Fig. 14, the minimized objective function value was 2.98 in the conventional method, whereas the minimized value was about 1.88 in the proposed method. Although the optimization had constraints on the robust stability for the proposed method, the performance factor of the proposed method was better than that of the conventional method. The results imply that the proposed structure can improve the performance of the control for the active power output of VPP.

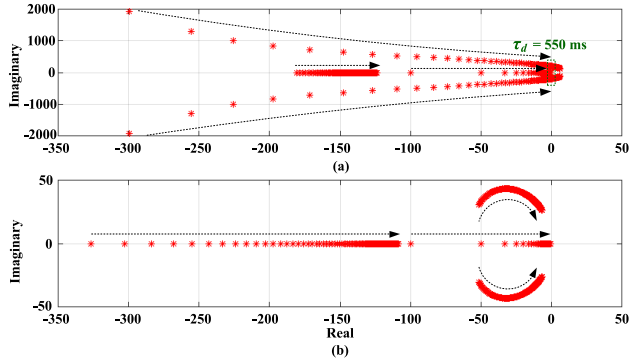

FIGURE 15. Dominant eigenvalues with varying communication delay from $\tau_d = 10$ ms to 2 s; (a) in the conventional method and (b) in the proposed method.

On the other hand, the stability of the system was analyzed when the communication speed varied from the nominal value, $\tau_d = 20$ ms. The stability of the system can be verified from the eigenvalues of the system matrix $\mathbf{A}$. The system is stable if and only if real parts of all eigenvalues have negative values. Figs. 15(a) and (b) show the dominant eigenvalues of the conventional and the proposed methods, when τ_d varied from 10 ms to 2 s. As shown in Fig. 15(a), if τ_d was over 550 ms, the system became unstable in the conventional method. However, as shown in Fig. 15(b), the system was maintained within the stable region regardless of varying τ_d in the proposed method.

From the results, we can conclude that the proposed FFC method for the active power of a VPP can improve the control performance and the robustness against the variation in communication speed.

C. CASE STUDY

Based on the test system, time-domain simulation was performed with Simulink/MATLAB for case study. The results

TABLE 2. Summarized proposals and the purpose of case study.

Proposals	Conventional method	Proposed method	Verification in case study
Consideration of DER characteristics	X	O	Case II
High-speed communication-free for active power control	X	O	
Central control unit-free for reactive power control	X	O	Case I

for Case I and Case II are presented when the power of REG at MPP was fluctuated from the predicted power ($P_{MPPT} \neq P_{REG,0} = 30$kW) as shown in Fig. 16. The purpose of simulations for Case I and Case II was to verify the proposals of this study, and is summarized as in Table 2.

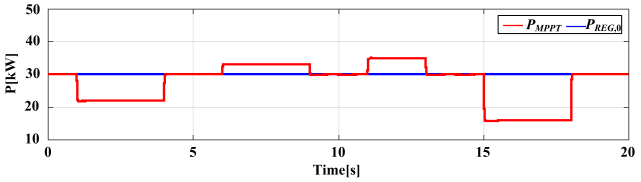

FIGURE 16. Active power at MPP and predicted active power of REG for case study.

1) CASE I

In Case I, failure of central control units occurred within a load variation scenario. Case I consists of Case I(a) and Case I(b). In Case I(a), allowable voltage range was determined as $V_{min} = 0.9$ p.u. and $V_{max} = 1.1$ p.u. In this case, the conventional method and entire proposed method were compared; thus, both active and reactive power controls were disabled in the conventional method and active power control was disabled in the proposed method. In Case I(b), the allowable voltage range was set as $V_{min} = 0.945$ p.u. and $V_{max} = 1.065$ p.u. In this case, to verify the effectiveness of the supplementary SPQ droop constant, K'_{SPQ}, simulation results of the proposed SPQ droop control methods with and without the use of K'_{SPQ} were compared.

– Case I(a)

In Case I(a), as P_{MPPT} varied, both the active and reactive power of an REG are presented as shown in Figs. 17(a) and (b), respectively. In both cases, the REG made the active power as P_{MPPT}. REG made the reactive power as the scheduled value in the conventional case, however, REG adjusted the reactive power from the scheduled value because of the SPQ droop controller in the proposed case.

Due to the variation in the active power of REG, the output of the VPP also varied as shown in Fig. 18. In both methods, as the variation in the active power of the REG deviated from the predicted value, the VPP was hard to maintain the power at the contracted value without central controllers; MTG and ESS kept their outputs as scheduled value as shown in Figs. 19 and 20. Furthermore, in the conventional case, although the reactive power of all devices was constant as

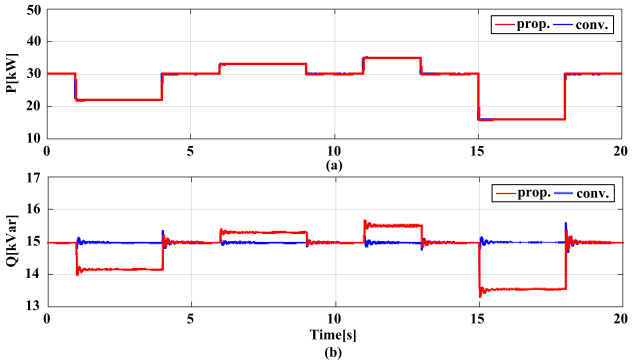

FIGURE 17. (a) Active power and (b) reactive power of REG in Case I(a).

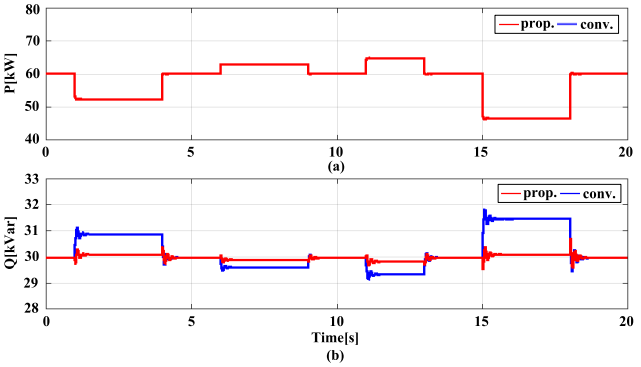

FIGURE 18. (a) Active power and (b) reactive power of VPP in Case I(a).

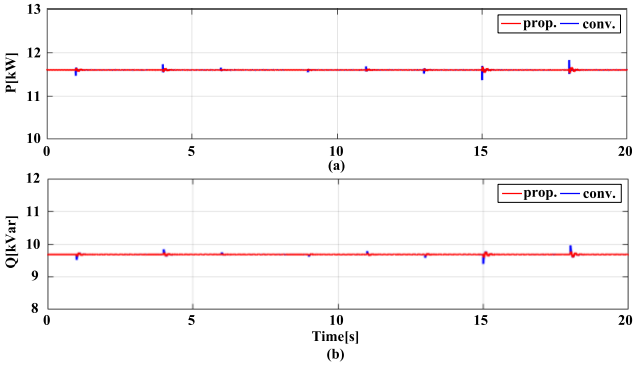

FIGURE 19. (a) Active power and (b) reactive power of MTG in Case I(a).

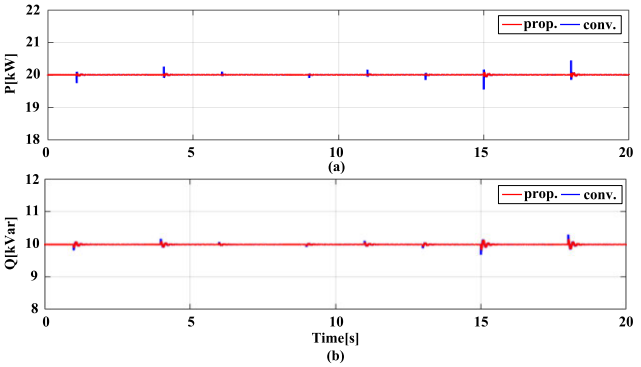

FIGURE 20. (a) Active power and (b) reactive power of ESS in Case I(a).

shown in Figs. 17(b), 19(b), and 20(b), the reactive power of the VPP varied because of the variation in the active power of

REG. However, in the proposed case, owing to the proposed SPQ droop controller, the reactive power of the VPP could be maintained at the contracted value without central control units. Fig. 21 shows the bus voltage of the REG. As the voltage could be within the allowable range (0.9 ∼ 1.1 p.u.) with K_{SPQ}, supplementary SPQ droop constant was not used (i.e. droop constant was fixed as K_{SPQ}); thus, the reactive power of VPP could be maintained in whole time periods.

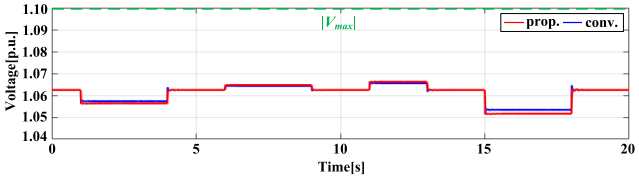

FIGURE 21. Voltage of REG-connected bus in Case I(a).

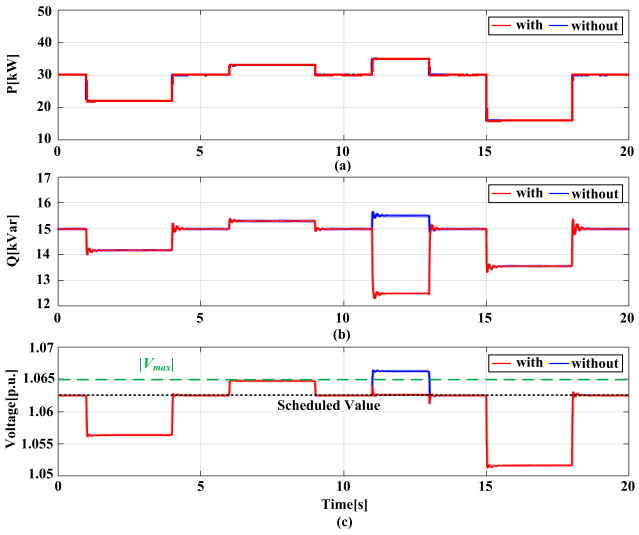

FIGURE 22. (a) Active power, (b) reactive power, and (c) bus voltage of REG in Case I(b).

– *Case I(b)*

In Case I(b), Figs. 22(a), (b), and (c) show the active power, reactive power, and bus voltage of the REG, respectively. As shown in Fig. 22(a), in both methods with and without the use of K'_{SPQ}, REG made the active power as P_{MPPT}.

Due to the variation in the active power of REG, the output of VPP also varied as shown in Fig. 23. In both methods with and without the use of K'_{SPQ}, as the variation in the active power of REG deviated from the predicted value, the VPP was hard to maintain the active power as the contracted value without central control units. However, regardless of the use of K'_{SPQ}, owing to the proposed SPQ droop control in both methods, the reactive power of VPP could be maintained as contracted value when the voltage remained within the allowable range, i.e., normal state, as shown in Fig. 23(b).

In the method without the use of K'_{SPQ}, the reactive power of VPP could be always maintained as the contracted value as shown in Fig. 23(b). However, the voltage deviated from the allowable range between 11 to 13 s as shown in Fig. 22(c). As the SPQ droop constant was fixed as K_{SPQ}, even though

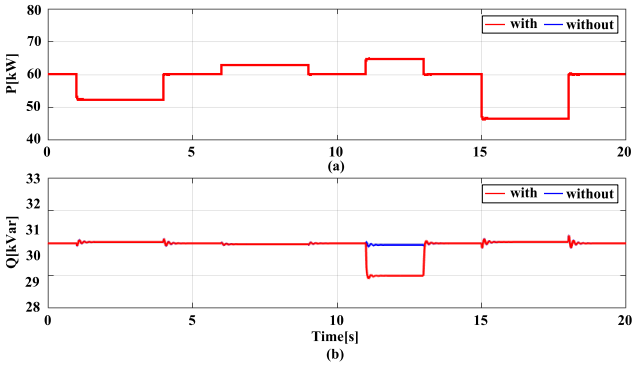

FIGURE 23. (a) Active power and (b) reactive power of VPP in Case I(b).

the voltage deviated away from the allowable range, the voltage control could not be controlled.

However, in the proposed method with the use of K'_{SPQ}, the voltage remained within the allowable range as shown in Fig. 22(c). Between 11 to 13 s, as (27) was not satisfied, the SPQ droop constant was changed from K_{SPQ} to K'_{SPQ}. Owing to K'_{SPQ}, the voltage was returned to the scheduled value between 11 to 13 s, as shown in Fig. 22(c). As the SPQ droop constant was K'_{SPQ} between 11 to 13, the reactive power of VPP could not be maintained as shown in Fig. 23(b). This phenomenon was inevitable because the voltage should be maintained within the allowable range. After 13 s, as the voltage could remain within the allowable range with K_{SPQ} (i.e., (27) is satisfied), the droop constant was changed from K'_{SPQ} to K_{SPQ} and the reactive power of VPP could be maintained as shown in Fig. 23(b).

In summary, with the entire local reactive power control including the proposed and supplementary SPQ droop constants, the reactive power of VPP could be maintained locally and the voltage was not allowed to deviate away from the allowable range simultaneously. Therefore, we can conclude that the proposed controller can reduce dependency on communications and improve system reliability while simultaneously achieving the control objectives.

2) CASE II

In Case II, communication was delayed within a load variation scenario; communication speed was delayed from $\tau_d = 20$ (nominal communication speed) to 300 ms at 5 s and delayed from $\tau_d = 300$ to 600 ms at 10 s. Here, the results from the proposed control method were compared to those from the conventional control method. Additionally, the allowable voltage range was determined as $V_{min} = 0.9$ p.u. and $V_{max} = 1.1$ p.u. and as the voltages were not deviated from the allowable range (i.e., (27) is satisfied), K'_{SPQ} was not used as in Case I(a).

Before 5 s, as shown in Fig. 24, according to the change in P_{MPPT}, the active and reactive power of the REG in both methods was similar as in Case I. However, as shown in Fig. 25, despite the variation in the output of the REG, the active and reactive power of the VPP can be tightly

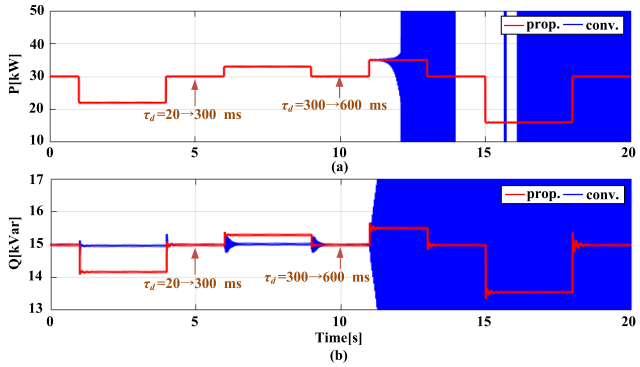

FIGURE 24. (a) Active power and (b) reactive power of REG in Case II.

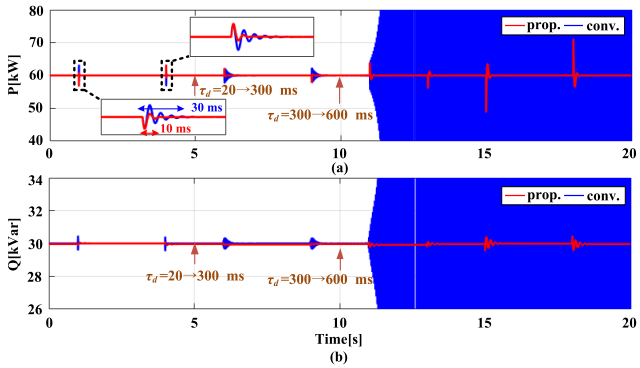

FIGURE 25. (a) Active power and (b) reactive power of VPP in Case II.

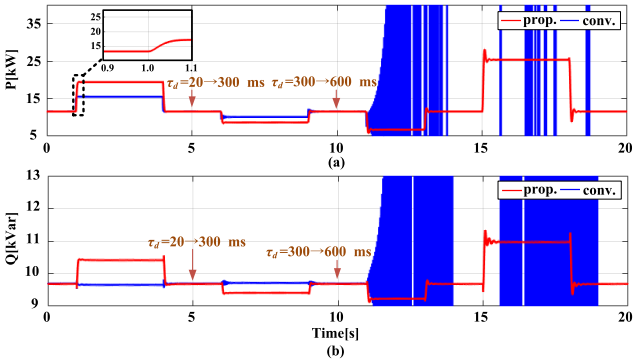

FIGURE 26. (a) Active power and (b) reactive power of MTG in Case II.

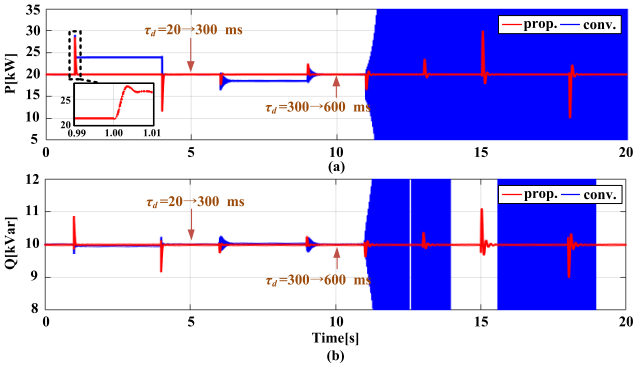

FIGURE 27. (a) Active power and (b) reactive power of ESS in Case II.

maintained at the contracted value in both methods. However, the detailed performance of the VPP output was different. As shown in the enlarged figures in Fig. 25 (a), the responses of the proposed method had less error than those of the conventional method. Those results correspond to the analysis in Fig. 14. Although the gains for both methods were optimally designed, the proposed method had better performance. Furthermore, it is notable that the proposed control method can maintain the reactive power of VPP locally without using central control unit.

After 5 s, still, the VPP output can be controlled in both methods. However, compared with the proposed method, the control performance significantly degrades in the conventional method due to the increasing communication delay. After 10 s, with the further delayed communication speed, the control system rapidly collapsed in the conventional method. This result corresponds to the stability analysis in Fig. 15, which implies that the conventional method is unstable when $\tau_d > 550$ ms. However, in the proposed method, the system did not collapse, as analyzed in Fig. 15 and the VPP output can be controlled.

Simultaneously, Figs. 26 and 27 present the output of MTG and ESS, respectively. In the conventional method, when the active power of the REG is fluctuated, both ESS and MTG participated in the FFC control equally at the steady-state. However, in the proposed method, the active power of the ESS was adjusted only at transient state and returned to the scheduled value at steady state. Meanwhile, the MTG slowly responded and the active power of the MTG was deviated from the scheduled value to maintain the active power of the VPP at the steady-state. In other words, ESS matched the instant power gap before MTG produced enough power. As shown in the enlarged figure of Fig. 26(a), to control the VPP output, MTG took about 100 ms to reach the steady state. While MTG required about 100 ms to increase the output power, ESS matched the power gap rapidly (about 10 ms) as shown in the enlarged figure of Fig. 27(a). Due to its faster response time, ESS covered the power gap instead of MTG. Thus, as shown in the enlarged figure of Fig. 25(a), the output of VPP (red line for the proposed control) could be maintained rapidly (about 10 ms) even when the output of REG was fluctuated. Considering that it took about 30 ms to saturate the output power of VPP in the conventional method as shown in Fig. 25(a), the coordination of DERs in the proposed method was more effective than that of the conventional method.

The results show that the coordination between the ESS and the MTG is performed effectively while considering the different characteristics of both the ESS and the MTG. In addition, the results imply that such coordination is the cause of the improved performance of the active power control for the VPP as presented in Fig. 25 (a).

From the coordination of the MTG and the ESS in the proposed structure of a centralized FFC for active power control of a VPP, the better performance and more efficient use of ESSs and MTGs can be obtained. Furthermore, the proposed

design method for the gains of the central active power controller presents the improved robustness against unexpected communication delay.

VI. CONCLUSION

A new FFC method for the VPP was proposed considering characteristics of various DERs and a reduction of the communication dependency. The active power of the VPP was maintained by the central PI controller using the proposed structure, which presents the method of allocating control signals to DERs and the design method of gains to have improved robustness against unexpected communication delay. Simultaneously, the reactive power of the VPP was managed by the proposed local controller called SPQ droop. Due to the entire proposed FFC for VPP, the control performance is improved and the control objective is achieved without the requirement for high-speed communication and extra central control unit(s), thus reducing communication dependency and system complexity.

The proposed control method will contribute greatly to further help the implementation and deployment of VPPs. However, the proposed control method was based on a VPP system in which the operator of the VPP manages all DERs and power system networks. The different type of VPP system, where the operator manages only DERs, has also appeared recently. Considering that the operator of such a VPP system lacks the relevant information about the power system networks, it is much more complicated to control the VPP output at the contracted value. Therefore, a new control method for the VPP output is required for such a VPP system, and it will be the focus of our future works.

APPENDIX A
STATE SPACE MODEL OF CONVENTIONAL METHOD

$$\dot{\mathbf{X}} = \mathbf{AX} + \mathbf{BU}, \tag{A1}$$
$$\mathbf{Y} = \mathbf{CX}, \tag{A2}$$

where,

$$\mathbf{X} = [\Delta P_{VPP}, \Delta P_{MTGs}, \Delta \dot{P}_{MTGs}, \Delta \ddot{P}_{MTGs}, \Delta P_{ESSs}, \Delta \dot{P}_{ESSs}, \Delta \ddot{P}_{ESSs}]^T,$$

$$\mathbf{U} = [\Delta \dot{P}_{REGs}], \mathbf{Y} = [\Delta P_{VPP}],$$

$$\mathbf{A} = \begin{bmatrix} 0 & 0 & 1 & 0 & 0 & 1 & 0 \\ 0 & 0 & 1 & 0 & 0 & 0 & 0 \\ 0 & 0 & 0 & 1 & 0 & 0 & 0 \\ a_1 & 0 & a_2 & a_3 & 0 & a_4 & 0 \\ 0 & 0 & 0 & 0 & 0 & 1 & 0 \\ 0 & 0 & 0 & 0 & 0 & 0 & 1 \\ a_5 & 0 & a_6 & 0 & 0 & a_7 & a_8 \end{bmatrix},$$

$$\mathbf{B} = \begin{bmatrix} 1 \\ 0 \\ 0 \\ 0 \\ 0 \\ 0 \\ 0 \end{bmatrix}, \quad \mathbf{C} = \begin{bmatrix} 1 \\ 0 \\ 0 \\ 0 \\ 0 \\ 0 \\ 0 \end{bmatrix}^T,$$

$$a_1 = -0.5k_i\tau_d^{-1}\tau_{MTG}^{-1}, a_2 = -(1+0.5k_p)\tau_d^{-1}\tau_{MTG}^{-1},$$
$$a_3 = -(\tau_d+\tau_d)\tau_d^{-1}\tau_{MTG}^{-1}, \ a_4 = -0.5k_p\tau_d^{-1}\tau_{MTG}^{-1},$$
$$a_5 = -0.5k_i\tau_d^{-1}\tau_{ESS}^{-1}, a_6 = -0.5k_p\tau_d^{-1}\tau_{ESS}^{-1},$$
$$a_7 = -(1+0.5k_p)\tau_d^{-1}\tau_{ESS}^{-1}, a_8 = -(\tau_d+\tau_d)\tau_d^{-1}\tau_{ESS}^{-1}.$$

REFERENCES

[1] H. Nezamabadi and M. Setayesh Nazar, "Arbitrage strategy of virtual power plants in energy, spinning reserve and reactive power markets," *IET Gener., Transmiss. Distrib.*, vol. 10, no. 3, pp. 750–763, Feb. 2016.
[2] T. L. Vandoorn, B. Zwaenepoel, J. D. M. De Kooning, B. Meersman, and L. Vandevelde, "Smart microgrids and virtual power plants in a hierarchical control structure," in *Proc. 2nd IEEE PES Int. Conf. Exhib. Innov. Smart Grid Technol.*, Dec. 2011, pp. 1–7.
[3] A. Baringo, L. Baringo, and J. M. Arroyo, "Day-ahead self-scheduling of a virtual power plant in energy and reserve electricity markets under uncertainty," *IEEE Trans. Power Syst.*, vol. 34, no. 3, pp. 1881–1894, May 2019.
[4] M. J. Kasaei, M. Gandomkar, and J. Nikoukar, "Optimal management of renewable energy sources by virtual power plant," *Renew. Energy*, vol. 114, pp. 1180–1188, Dec. 2017.
[5] H. Khan, V. Sreeram, S. Dasouki, Y. Mishra, and H. H. C. Iu, "Universal active and reactive power control of electronically interfaced distributed generation sources in virtual power plants operating in grid-connected and islanding modes," *IET Gener., Transmiss. Distrib.*, vol. 7, no. 8, pp. 885–897, Aug. 2013.
[6] S.-J. Ahn, J.-W. Park, I.-Y. Chung, S.-I. Moon, S.-H. Kang, and S.-R. Nam, "Power-sharing method of multiple distributed generators considering control modes and configurations of a microgrid," *IEEE Trans. Power Del.*, vol. 25, no. 3, pp. 2007–2016, Jul. 2010.
[7] O. Palizban, K. Kauhaniemi, and J. M. Guerrero, "Microgrids in active network management—Part I: Hierarchical control, energy storage, virtual power plants, and market participation," *Renew. Sustain. Energy Rev.*, vol. 36, pp. 428–439, Aug. 2014.
[8] V. Ravikumar Pandi, A. Al-Hinai, and A. Feliachi, "Adaptive coordinated feeder flow control in distribution system with the support of distributed energy resources," *Int. J. Electr. Power Energy Syst.*, vol. 85, pp. 190–199, Feb. 2017.
[9] N. Etherden, V. Vyatkin, and M. H. J. Bollen, "Virtual power plant for grid services using IEC 61850," *IEEE Trans. Ind. Informat.*, vol. 12, no. 1, pp. 437–447, Feb. 2016.
[10] X. Lei, T. Huang, Y. Yang, Y. Fang, and P. Wang, "A bi-layer multi-time coordination method for optimal generation and reserve schedule and dispatch of a grid-connected microgrid," *IEEE Access*, vol. 7, pp. 44010–44020, 2019.
[11] B. Mohandes, M. S. E. Moursi, N. Hatziargyriou, and S. E. Khatib, "A review of power system flexibility with high penetration of renewables," *IEEE Trans. Power Syst.*, vol. 34, no. 4, pp. 3140–3155, Jul. 2019.
[12] J. Shen, C. Jiang, Y. Liu, and X. Wang, "A microgrid energy management system and risk management under an electricity market environment," *IEEE Access*, vol. 4, pp. 2349–2356, 2016.
[13] S. Xia, Z. Ding, T. Du, D. Zhang, M. Shahidehpour, and T. Ding, "Multitime scale coordinated scheduling for the combined system of wind power, photovoltaic, thermal generator, hydro pumped storage, and batteries," *IEEE Trans. Ind. Appl.*, vol. 56, no. 3, pp. 2227–2237, Jun. 2020.
[14] Y.-S. Kim, E.-S. Kim, and S.-I. Moon, "Frequency and voltage control strategy of standalone microgrids with high penetration of intermittent renewable generation systems," *IEEE Trans. Power Syst.*, vol. 31, no. 1, pp. 718–728, Jan. 2016.

[15] J.-W. Chang, G.-S. Lee, H.-J. Moon, M. B. Glick, and S.-I. Moon, "Coordinated frequency and State-of-Charge control with multi-battery energy storage systems and diesel generators in an isolated microgrid," *Energies*, vol. 12, no. 9, p. 1614, Apr. 2019.

[16] J. Pahasa and I. Ngamroo, "Coordinated PHEV, PV, and ESS for microgrid frequency regulation using centralized model predictive control considering variation of PHEV number," *IEEE Access*, vol. 6, pp. 69151–69161, 2018.

[17] M. Shafiekhani, A. Badri, M. Shafie-khah, and J. P. S. Catalão, "Strategic bidding of virtual power plant in energy markets: A bi-level multi-objective approach," *Int. J. Electr. Power Energy Syst.*, vol. 113, pp. 208–219, Dec. 2019.

[18] H. Pandžić, I. Kuzle, and T. Capuder, "Virtual power plant mid-term dispatch optimization," *Appl. Energy*, vol. 101, pp. 134–141, Jan. 2013.

[19] D. Pudjianto, C. Ramsay, and G. Strbac, "Virtual power plant and system integration of distributed energy resources," *IET Renew. Power Gener.*, vol. 1, no. 1, pp. 10–16, Mar. 2007.

[20] G.-Y. Lee, B.-S. Ko, J. Cho, and R.-Y. Kim, "A distributed control method based on a voltage sensitivity matrix in DC microgrids with low-speed communication," *IEEE Trans. Smart Grid*, vol. 10, no. 4, pp. 3809–3817, Jul. 2019.

[21] D. E. Olivares, A. Mehrizi-Sani, A. H. Etemadi, C. A. Cañizares, R. Iravani, M. Kazerani, A. H. Hajimiragha, O. Gomis-Bellmunt, M. Saeedifard, R. Palma-Behnke, G. A. Jiménez-Estévez, and N. D. Hatziargyriou, "Trends in microgrid control," *IEEE Trans. Smart Grid*, vol. 5, no. 4, pp. 1905–1919, Jul. 2014.

[22] E. A. A. Coelho, D. Wu, J. M. Guerrero, J. C. Vasquez, T. Dragicevic, C. Stefanovic, and P. Popovski, "Small-signal analysis of the microgrid secondary control considering a communication time delay," *IEEE Trans. Ind. Electron.*, vol. 63, no. 10, pp. 6257–6269, Oct. 2016.

[23] C. J. Ramlal, A. Singh, S. Rocke, and M. Sutherland, "Decentralized fuzzy H_∞-iterative learning LFC with time-varying communication delays and parametric uncertainties," *IEEE Trans. Power Syst.*, vol. 34, no. 6, pp. 4718–4727, Nov. 2019.

[24] W. W. A. G. da Silva, T. R. Oliveira, and P. F. Donoso-Garcia, "Hybrid distributed and decentralized secondary control strategy to attain accurate power sharing and improved voltage restoration in DC microgrids," *IEEE Trans. Power Electron.*, vol. 35, no. 6, pp. 6458–6469, Jun. 2020.

[25] Y. Khayat, M. Naderi, Q. Shafiee, Y. Batmani, M. Fathi, J. M. Guerrero, and H. Bevrani, "Decentralized optimal frequency control in autonomous microgrids," *IEEE Trans. Power Syst.*, vol. 34, no. 3, pp. 2345–2353, May 2019.

[26] M. Chen, X. Xiao, and J. M. Guerrero, "Secondary restoration control of islanded microgrids with a decentralized event-triggered strategy," *IEEE Trans. Ind. Informat.*, vol. 14, no. 9, pp. 3870–3880, Sep. 2018.

[27] N. L. Diaz, A. C. Luna, J. C. Vasquez, and J. M. Guerrero, "Centralized control architecture for coordination of distributed renewable generation and energy storage in islanded AC microgrids," *IEEE Trans. Power Electron.*, vol. 32, no. 7, pp. 5202–5213, Jul. 2017.

[28] P. WeBkamp, P. HauBmann, and J. Melbert, "600-A test system for aging analysis of automotive li-ion cells with high resolution and wide bandwidth," *IEEE Trans. Instrum. Meas.*, vol. 65, no. 7, pp. 1651–1660, Jul. 2016.

[29] F.-S. Pai, "An improved utility interface for microturbine generation system with stand-alone operation capabilities," *IEEE Trans. Ind. Electron.*, vol. 53, no. 5, pp. 1529–1537, Oct. 2006.

[30] H. Nikkhajoei, M. Saeedifard, and R. Iravani, "A three-level converter based micro-turbine distributed generation system," in *Proc. IEEE Power Eng. Soc. General Meeting*, Jun. 2006, pp. 18–22.

[31] L. Wang and G.-Z. Zheng, "Analysis of a microturbine generator system connected to a distribution system through power-electronics converters," *IEEE Trans. Sustain. Energy*, vol. 2, no. 2, pp. 159–166, Apr. 2011.

[32] A. Yazdani and R. Iravani, *Voltage-Sourced Converters in Power Systems: Modeling, Control, and Applications*. New York, NY, USA: Wiley, 2010.

[33] Y.-X. Dai, H. Wang, and G.-Q. Zeng, "Double closed-loop PI control of three-phase inverters by binary-coded extremal optimization," *IEEE Access*, vol. 4, pp. 7621–7632, 2016.

[34] I.-Y. Chung, W. Liu, D. A. Cartes, and K. Schoder, "Control parameter optimization for a microgrid system using particle swarm optimization," in *Proc. IEEE Int. Conf. Sustain. Energy Technol.*, Singapore, Nov. 2008, pp. 837–842.

[35] C. S. Ali Nandar, "Robust PI control of smart controllable load for frequency stabilization of microgrid power system," *Renew. Energy*, vol. 56, pp. 16–23, Aug. 2013.

[36] M. Saejia and I. Ngamroo, "Wide area robust TCSC controller design considering communication delay uncertainty," in *Proc. Int. Conf. Electr. Eng., Electron., Comput., Telecommun. Inf. Technol. (ECTI)*, Chiang Mai, Thailand, 2010, pp. 996–1000.

[37] M. M. J. Van De Wal, "Actuator control with H-infinity and mu-synthesis," Technische Universiteit Eindhoven, Eindhoven, The Netherlands, Tech. Rep., 1995. [Online]. Available: https://www.narcis.nl/publication/RecordID/oai:pure.tue.nl:publications%2Fb080305d-f636-4520-b099-c3938fcdf775

[38] K. Sabzevari, S. Karimi, F. Khosravi, and H. Abdi, "A novel partial transient active-reactive power coupling method for reactive power sharing," *Int. J. Electr. Power Energy Syst.*, vol. 113, pp. 758–771, Dec. 2019.

[39] J.-O. Lee, Y.-S. Kim, E.-S. Kim, and S.-I. Moon, "Generation adjustment method based on bus-dependent participation factor," *IEEE Trans. Power Syst.*, vol. 33, no. 2, pp. 1959–1969, Mar. 2018.

[40] F. Valenciaga and P. F. Puleston, "Supervisor control for a stand-alone hybrid generation system using wind and photovoltaic energy," *IEEE Trans. Energy Convers.*, vol. 20, no. 2, pp. 398–405, Jun. 2005.

[41] S. Mishra, G. Mallesham, and A. N. Jha, "Design of controller and communication for frequency regulation of a smart microgrid," *IET, Renew. Power Gener.*, vol. 6, no. 4, pp. 248–258, Jul. 2012.

[42] Y. C. Chen, J. Wang, A. D. Dominguez-Garcia, and P. W. Sauer, "Measurement-based estimation of the power flow jacobian matrix," *IEEE Trans. Smart Grid*, vol. 7, no. 5, pp. 2507–2515, Sep. 2016.

[43] X. Wang, J. W. Bialek, and K. Turitsyn, "PMU-based estimation of dynamic state jacobian matrix and dynamic system state matrix in ambient conditions," *IEEE Trans. Power Syst.*, vol. 33, no. 1, pp. 681–690, Jan. 2018.

[44] S. Papathanassiou, N. Hatziargyriou, and K. Strunz, "A benchmark low voltage microgrid network," in *Proc. Symp. Power Syst. Dispersed Generat., Technol., Impact Develop. Oper. Perform. (CIGRE)*, Apr. 2005, pp. 1–8.

JAE-WON CHANG (Student Member, IEEE) received the B.S. degree in electrical and computer engineering from Seoul National University, Seoul, South Korea, in 2015, where he is currently pursuing the Ph.D. degree in electrical and computer engineering. His research interests include distributed generation, energy storage systems, microgrids, and virtual power plant.

HEE SEUNG MOON (Student Member, IEEE) received the B.S. degree in electrical and computer engineering from Seoul National University, Seoul, South Korea, in 2016, where he is currently pursuing the Ph.D. degree in electrical and computer engineering. His research interests include power economics, distribution system operation, balancing cost, and virtual power plant.

SEUNG-IL MOON (Senior Member, IEEE) received the B.S. degree in electrical engineering from Seoul National University, Seoul, South Korea, in 1985, and the M.S. and Ph.D. degrees in electrical engineering from Ohio State University, Columbus, OH, USA, in 1989 and 1993, respectively. He is currently a Professor with the School of Electrical and Computer Engineering, Seoul National University. His research interests include power system operation, power quality, HVDC systems, renewable energy, and distributed generation. He was a recipient of several awards and honors, including the Service Merit Medal (Korean Government), the Young-Moon Park Best Scholar Award, and the Outstanding Scholar Award (Korean Institute of Electrical Engineers).

YONG TAE YOON (Member, IEEE) received the B.S., M.Eng., and Ph.D. degrees from M.I.T., Cambridge, MA, USA, in 1995, 1997, and 2001, respectively. He is currently a Professor with the Department of Electrical and Computer Engineering, Seoul National University, Seoul, South Korea. His research interests include power economics, smart grid/microgrid, and decentralized operation.

MARK B. GLICK (Member, IEEE) received the B.A. degree in mathematics from Lamar University, in 1983, and the M.S. degree in public management and policy from Carnegie-Mellon University, in 1986. He is currently a Faculty Specialist on energy policy with the Hawaii Natural Energy Institute, where he has developed a practice focused on energy transitions and associated innovation-based economic growth in Hawaii and the Asia Pacific region. Previously, he was a Hawaii State Energy Administrator and was directly involved in drafting and supporting passage of the nation's first 100 percent renewable portfolio standard. He also established the $150 million Green Energy Market Securitization (GEMS) and GreenSun Hawaii loan programs, and served as Vice Chair of the National Association of State Energy Officials (NASEO).

SEUNG WAN KIM (Member, IEEE) received the B.S. and Ph.D. degrees in electrical engineering from Seoul National University, Seoul, South Korea, in 2012 and 2018, respectively. He is currently an Assistant Professor with the Department of Electrical Engineering, Chungnam National University, Daejeon, South Korea. His research interests include energy policy and electricity market design.